Measurements of stiff-material compliance on the nanoscale using ultrasonic force microscopy

F. Dinelli*
Department of Materials, University of Oxford, Parks Road, OX1 3PH Oxford, United Kingdom

S. K. Biswas
Indian Institute of Science, Bangalore, India

G. A. D. Briggs and O. V. Kolosov†
Department of Materials, University of Oxford, Parks Road, OX1 3PH Oxford, United Kingdom
(Received 14 May 1999; revised manuscript received 28 December 1999)

Ultrasonic force microscopy (UFM) was introduced to probe nanoscale mechanical properties of stiff materials. This was achieved by vibrating the sample far above the first resonance of the probing atomic force microscope cantilever where the cantilever becomes dynamically rigid. By operating UFM at different set force values, it is possible to directly measure the absolute values of the tip-surface contact stiffness. From this an evaluation of surface elastic properties can be carried out assuming a suitable solid-solid contact model. In this paper we present curves of stiffness as a function of the normal load in the range of 0–300 nN. The dependence of stiffness on the relative humidity has also been investigated. Materials with different elastic constants (such as sapphire lithium fluoride, and silicon) have been successfully differentiated. Continuum mechanics models cannot however explain the dependence of stiffness on the normal force and on the relative humidity. In this high-frequency regime, it is likely that viscous forces might play an important role modifying the tip-surface interaction. Plastic deformation might also occur due to the high strain rates applied when ultrasonically vibrating the sample. Another possible cause of these discrepancies might be the presence of water in between the two bodies in contact organizing in a solidlike way and partially sustaining the load.

I. INTRODUCTION

The invention and development of the atomic force microscope[1] (AFM) has supplied a new powerful means of surface investigation. Provided the probe is sharp enough, AFM can reproduce surface topography with a lateral resolution of less than a few nanometers and a vertical resolution of better than 1 Å.[2] Various AFM modifications (such as so-called force modulation microscopes) can map surface elastic properties while simultaneously probing the topography.[3,4] However, these force modulation techniques are limited in stiffness sensitivity by the probe spring constant, typically of the order of a few N/m.[5] While not precluding investigations and quantitative evaluation of elastic properties of polymers and compliant materials, this is extremely limiting in the case of relatively stiff materials ($E > 50$ GPa). In fact, even at a normal load of a few nanoNewtons, the tip-surface contact stiffness is expected to be in the range of hundreds of N/m. One way to overcome this limitation is to apply a magnetic force directly to the tip.[6,7] The upper limit in stiffness is then determined by the detection sensitivity to the normal deflection. However, at the moment this method is not applicable to very stiff materials and the limitation still persists.[8]

Another approach to investigate stiff materials is to use high-frequency modulation above the first cantilever resonance and to exploit the fact that the cantilever becomes dynamically rigid.[9] Techniques based on this idea are the ultrasonic force microscopy[10] (UFM), the scanning local acceleration microscopy,[11] and the atomic force acoustic microscopy.[12] In particular, UFM relies on the nonlinearity of the tip-surface interaction to detect the high-frequency force modulation. The upper limit in stiffness is now given by the effective cantilever stiffness at the excitation frequency and can be several orders of magnitude higher than the quasistatic value.

In 1993, Kolosov and Yamanaka[10] proposed a method to measure the contact stiffness and from that to evaluate the sample elastic modulus by using a suitable contact mechanics model: the ''differential UFM.'' This method can be particularly helpful as it provides direct stiffness measurements independent of the details of the contact mechanics. In this paper we would like to address the applicability of the differential UFM to a quantitative analysis of surface elastic properties. Materials with different elastic properties have been investigated in different environmental conditions. The experimental data and the predictions of continuum mechanics models are compared and discussed.

II. UFM DETECTION AND DIFFERENTIAL UFM

In order to understand the UFM detection and the differential UFM let us start by considering the nonlinearity of the tip-surface interaction and what happens when the indentation is modulated at high frequency. In Fig. 1 a schematic force-indentation curve is plotted.[13] In general we find that once the tip and the surface are in contact, if one tries to pull them apart or to push them together the behavior is different. There is a strong nonlinearity. If the normal force is initially set at a certain value F_1 and one starts modulating the indentation, e.g., sinusoidally around this point, the force averaged over one modulation cycle depends dramatically on the

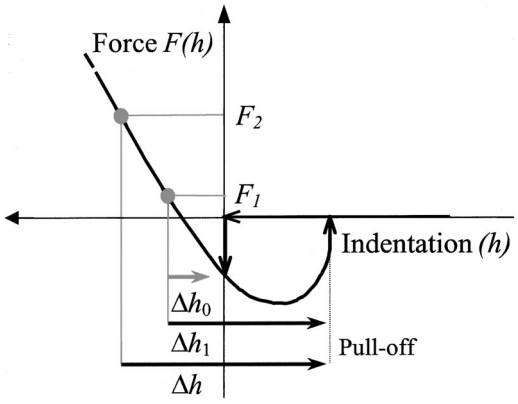

FIG. 1. Schematic of a force-indentation curve. For a normal force value set to F_1, modulating the indentation by Δh_0 the normal force averaged over one modulation cycle is almost unchanged. Δh_1 is the indentation variation needed to reach the pull-off point and change dramatically the average normal force. If the normal force is set to $F_2 > F_1$, an indentation variation $\Delta h_2 > \Delta h_1$ is needed to reach the pull-off point.

modulation amplitude. If the variation is equal to Δh_0, the normal force does not change appreciably. An indentation variation of Δh_1 is needed to reach the pull-off point where the nonlinearity is pronounced and the normal force varies strongly. If the normal force is set to $F_2 > F_1$, an indentation variation $\Delta h_2 > \Delta h_1$ is needed to reach the pull-off point.

In the case of stiff samples the indentation cannot be much varied by modulating the tip-surface distance at a frequency below the main resonant frequency of the cantilever.[14] A significant modulation of the indentation can only be achieved via an out-of-plane vibration of the sample at a frequency far above the main resonance of the cantilever.[10] At this frequency, the cantilever vibration response to an ultrasonic amplitude a can be considered negligible and therefore $a \cong \Delta h$. In practice the cantilever spring constant is increased working in the inertial regime. High normal and lateral force sensitivities are however maintained for quasistatic variations.

UFM is implemented by introducing a piezoplate underneath the sample to allow out-of-plane vibration in the MHz range, typically above 2 MHz. The quasistatic normal deflection is monitored as a function of the ultrasonic amplitude (Fig. 2). For $a_0 = \Delta h_0$, no variation in normal force is expected. When the ultrasonic amplitude is high enough to reach the pull-off point ($a_1 = \Delta h_1$), the contact is broken for part of the ultrasonic cycle and the time-averaged force shows a discontinuity. We will refer to this ultrasonic amplitude value as the ''threshold amplitude.'' The normal deflection reflects this discontinuity in force with a jump. We shall call this discontinuity in normal deflection the ''force jump'' [Fig. 2(b)]. Any further increase of the ultrasonic amplitude results in a continuous increase of the time-averaged force and therefore of the quasistatic normal deflection. The normal force modified by the ultrasonic vibration can be defined as a function $F_m(h_1, a)$ dependent on the initial indentation h_1 and the ultrasonic amplitude a. The new force F_m can be calculated as follows:

$$F_m(h_1, a) = \frac{1}{T_{\text{ult}}} \int_{T_{\text{ult}}} F[h_1 - a\cos(2\pi f_{\text{ult}} t)]\, dt, \qquad (1)$$

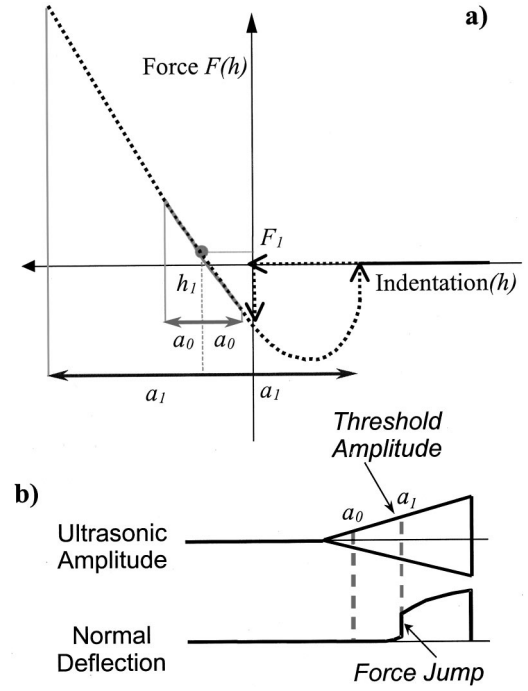

FIG. 2. Applying an out-of-plane vibration of amplitude a to the sample at a frequency at which the cantilever response is negligible, one can actually modulate the tip-surface indentation ($a = \Delta h$) and, therefore, be sensitive to the nonlinearity of the force-indentation curve. (a) For small ultrasonic amplitudes such as a_0, the normal force averaged in time over one ultrasonic period [Eq. (1)] is equal to the initial value F_1 as the force curve is linear in first approximation. For the threshold amplitude a_1, the average normal force (averaged over the broken line) has a discontinuity that depends on the *adhesion hysteresis*. The contact is broken for part of the ultrasonic cycle. (b) Schematic normal deflection response induced by an out-of-plane ultrasonic vibration of the sample. There is a variation of the normal deflection only for ultrasonic amplitudes higher than the threshold amplitude a_1. At this value, a discontinuity occurs in the normal force and normal deflection (force jump).

where $F(h)$ is the force dependence on the indentation depth without ultrasonic vibration; f_{ult} is the ultrasonic frequency; the integral is taken over a period $T_{\text{ult}} = 1/f_{\text{ult}}$.[10] When F_m increases due to the nonlinearity, the cantilever deflection increases as well until a new equilibrium position is reached. This new stationary normal deflection is given by

$$F_m(h_{\text{eq}}, a) = k_C z_{\text{eq}}, \qquad (2)$$

where z_{eq} and h_{eq} are the new cantilever deflection and sample indentation depth, respectively.

Summarizing, the ultrasonic vibration of the sample can be detected due to the nonlinearity of the force-indentation curve. In a real experiment a feedback circuit is active, and the normal deflection is corrected to maintain the value initially set. Thus the simple addition of an ultrasonic vibration has no effect. One needs to detect the normal deflection variation due to the ''ultrasonic force'' acting on the tip [Fig. 2(b)]. This can be done if the ultrasonic vibration is modulated in amplitude at a frequency higher than the feedback cutoff frequency. This prevents the feedback from correcting variations of the normal deflection. For our commercial system, it has been found that the cutoff frequency is equal to

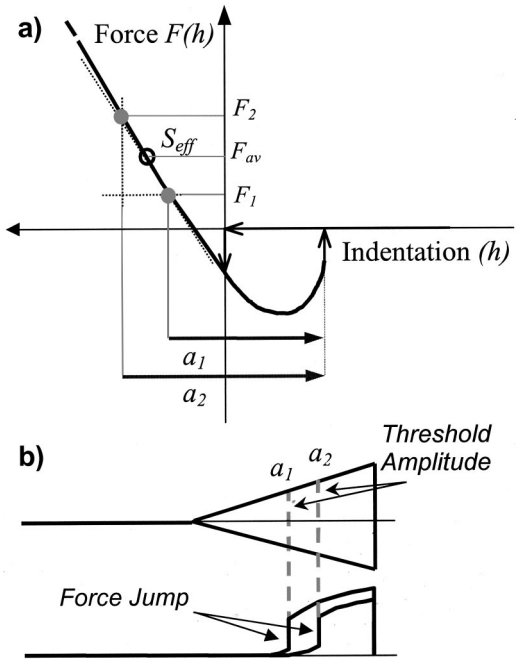

FIG. 3. (a) Measuring the threshold amplitudes a_i $(i=1,2)$ at two different values of normal force F_i $(i=1,2)$, the contact stiffness S_{eff} can be evaluated using Eq. (3). (b) Schematic of the ultrasonic deflection for two normal forces. A force jump occurs in correspondence to the threshold amplitude.

0.5 kHz for loop-gain values typically employed. However this cutoff value can be further reduced by reducing the loop gain whose choice is strongly dependent on the scan speed. The feedback error signal is then used to monitor the ''ultrasonic deflection.''

The shape of the force-indentation curve depends on surface adhesive and elastic properties. In particular, the *adhesion hysteresis* and the slope of the curve in the repulsive regime are affected, respectively. Variations in these parameters change the shape of the ultrasonic deflection. Conversely variations in the shape of the ultrasonic deflection contain information on surface adhesive and elastic properties. From Fig. 1 it is also clear that the threshold amplitude should depend on the normal force value. For instance, the threshold amplitude $a(F_2)=a_2$ should be higher than the threshold amplitude $a(F_1)=a_1$. In Fig. 3 the basic principle of the differential UFM is schematically shown.[15] If one measures the threshold amplitude values (a_1 and a_2) for two different normal force values (F_1 and F_2), an effective contact stiffness S_{eff} can be operatively obtained as follows:

$$S_{\text{eff}}(F_{\text{av}})=\frac{F_2-F_1}{a_2-a_1}, \tag{3}$$

$$F_{\text{av}}=(F_2+F_1)/2. \tag{4}$$

$S_{\text{eff}}/(F_{\text{av}})$ is equal to the contact stiffness $S(F_{\text{av}})$ for $F_1 \rightarrow F_2$.

The differential UFM is based on three main assumptions.

(1) It is possible to identify a threshold amplitude. This threshold amplitude has been defined as the amplitude at which the contact starts breaking for part of the ultrasonic cycle (pull off). It can be identified as the amplitude at which a force jump occurs in the normal deflection signal.

(2) The point of contact instability (pull off) does not depend on the applied normal force.

(3) The cantilever vibration at the ultrasonic working frequency is negligible. Therefore the difference in threshold amplitude at two normal force values Δa can be equalled to the difference in indentation Δh.

These assumptions need a few notes of discussion. The first assumption is based on a clear identification of the threshold amplitude. This is easy in principle for a contact that presents an adhesion hysteresis (a clear force jump can be observed), less easy in the case of a contact that does not present an adhesion hysteresis. In practice, as we shall see, this problem needs further discussion in order to define unambiguous criteria for measuring the threshold amplitude.

The second assumption is based on assuming contact mechanics models that are only valid in quasistatic conditions. Viscoelastic effects that might influence the instability point (pull off), adhesion hysteresis, and more generally the whole shape of the force-indentation curve are assumed to be negligible. Plasticity is supposed to be absent.

The third assumption is based on the basis of representing the cantilever with a point-mass model. The authors did not have direct means to measure the linear response to the cantilever to the ultrasonic excitation. Recently Rabe, Janser, and Arnold built a heterodyne interferometer to measure the cantilever linear response.[16] Up to now, this group has not carried out dedicated experiments to measure simultaneously linear and nonlinear responses. However, using a distributed mass model, they have performed simulations that indicate that this ratio is relatively small and in many cases less than 0.05.[17] Therefore the approximation of a dynamically static cantilever is a reasonable one. It should be noted that these values are mainly useful as estimates of the high-frequency vibration response. They are valid for a rectangular cantilever, at a frequency not coinciding with a higher-order resonance, and for a damped contact.

III. CONTINUUM MECHANICS MODELS OF AN ELASTIC CONTACT

The connective link between values measured using the differential UFM and material elastic properties (such as Young's modulus) is the contact mechanics of the tip-surface system. Theories based on the continuum mechanics, that is no molecular or atomic structure is taken into account, are quite developed. It is still debated whether or not continuum mechanics is applicable on the scale of an AFM contact. However, molecular-dynamics calculations have shown that the broad conclusions are not greatly changed until only a few atoms are involved.[18]

Hertz in 1882 and Boussinesq in 1885 first treated the elastic contact of a punch and a flat surface.[19,20] These models consider only pure elastic deformations and no attractive force between the two bodies is included. For the Hertzian model, the radius of the contact area r_c between two spheres is given by

$$r_c^3=\frac{3FR^*}{4E_r}, \tag{5}$$

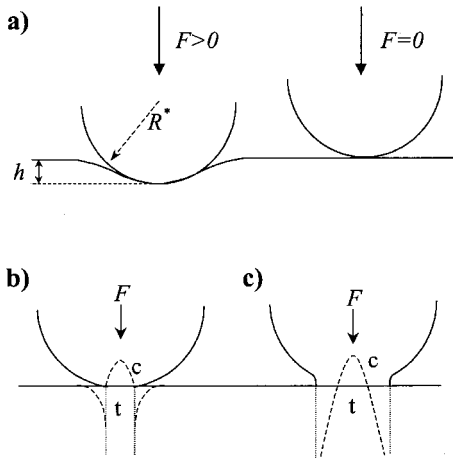

FIG. 4. (a) Hertzian contact: a sphere on a flat (infinitely stiff sphere in this case). No adhesive force between the tip and the surface is taken into account. At zero force no elastic deformation of the two bodies takes place. Models taking attractive forces into account. Interfacial stress for (b) DMT model; (c) JKR model. Tensile stress, **t**. Compressive stress, **c**. At pull off the predicted contact area is zero for the DMT model and nonzero for the JKR model.

$$\frac{1}{R^*}=\frac{1}{R_1}+\frac{1}{R_2}, \tag{6}$$

$$\frac{1}{E_r}=\frac{1-\nu_T^2}{E_T}+\frac{1-\nu_S^2}{E_S}, \tag{7}$$

where R^* is the reduced radius; R_1 and R_2 are the radii of the two spheres; E_r is the reduced Young's modulus; E_T and E_S are the tip and the sample Young's modulus, respectively; ν_T and ν_s are the tip and the sample Poisson's ratios; F is the normal force. (See Fig. 4.)

The indentation depth h is given by

$$h^3=\frac{9F^2}{16E_r^2R^*}. \tag{8}$$

In order to consider attractive forces, the Johnson-Kendall-Roberts[21] (JKR) and the Derjaguin-Muller-Toporov[22,23] (DMT) models were then introduced. More recently, Maugis and Barquins obtained general equations that, in the two limiting cases, reduce to the JKR and DMT equations.[24] Unfortunately, these equations can only be solved analytically in the two limiting cases. Maugis and Barquins also introduced a parameter λ that determines if a tip-surface system is better described by a JKR or by a DMT model:

$$\lambda=\frac{2\Delta\gamma/z_0}{\sqrt[3]{16\pi\Delta\gamma E_r^2/9R^*}}, \tag{9}$$

where z_0 is the equilibrium separation of the atoms; $\Delta\gamma$ is the Dupré work of adhesion.[25]

It turns out that if $\lambda>1$ then that particular system is better described by the JKR model; otherwise it is the DMT model that gives a better description. More specifically, the JKR model is more appropriate for a low elastic modulus, high adhesion, and large tip radii. On the other hand, the DMT model is more appropriate for small tip radii, low adhesion, and a high elastic modulus.

For the JKR case, the radius of the contact area r_c between two spheres is given by

$$r_c^3=\frac{3R^*}{4E_r}\{F+3\Delta\gamma\pi R^*+[6\Delta\gamma\pi R^*F+(3\Delta\gamma\pi R^*)^2]^{1/2}\}. \tag{10}$$

The work of adhesion is given by the following:[25]

$$\Delta\gamma=\gamma_1+\gamma_2-\gamma_{12}, \tag{11}$$

where γ_i $(i=1,2)$ is the free energy change when the surface area of a medium (in this case, the two surfaces in contact) is increased by unit area; γ_{12} is the energy necessary to create a unit area interface between the two surfaces considered.

The indentation depth h is equal to

$$h=\frac{r^2}{R^*}\left[1-\frac{2}{3}\left(\frac{r_0}{r}\right)^{3/2}\right], \tag{12}$$

where r_0 is the contact radius at zero normal force and is equal to

$$r_0^2=\frac{6\Delta\gamma\pi R^{*2}}{E_r}. \tag{13}$$

The DMT equations can be obtained from the Hertzian equations (5) and (8) simply by shifting the force dependence of an offset equal to the DMT pull-off force F_c:[26]

$$r_c^3=\frac{3(F+F_c)R^*}{4E_r}, \tag{14}$$

$$h^3=\frac{9(F+F_c)^2}{16E_r^2R^*}. \tag{15}$$

Using Eq. (8) and differentiating F with respect to h, one obtains for the contact stiffness S_{Hertz}:

$$S_{\mathrm{Hertz}}=6F^{1/3}R^*E_r^2. \tag{16}$$

Using Eqs. (10) and (12), the JKR contact stiffness is equal to

$$S_{\mathrm{JKR}}=\frac{\partial F}{\partial h}=\frac{F_c}{M_c}\frac{3^{2/3}A^{1/3}}{(2+B)A+\left(2\dfrac{F}{F_c}+A\right)B}, \tag{17}$$

where

$$A=2\left(1+\frac{F}{F_c}\right)^{1/2}+\frac{F}{F_c}+2, \tag{18}$$

$$B=1+\frac{1}{\left(1+\dfrac{F}{F_c}\right)^{1/2}}, \tag{19}$$

$$M_c=\frac{3}{4}\left(\frac{F_c^2}{16E_r^2R^*}\right)^{1/3}. \tag{20}$$

The DMT stiffness can be easily derived from the Hertzian stiffness by simply introducing a force offset equal to the pull-off force.

A. Further considerations

In an ambient environment the problem of two bodies contact is more complex. In general, surfaces are covered with a water film and organic contaminants. An exposure of a few minutes to air is sufficient for a surface to be covered with a layer of hydrocarbons. Even in the absence of organic contamination, when two surfaces approach each other water condenses and a water meniscus forms.[27] The problem of two spheres in an ambient environment was first tackled by Fogden and White.[28] This model, called the generalized Hertzian model, yields the following results.

(1) Large curvature radii and compliant spheres in an environment with low values of the relative humidity behave like a JKR system.

(2) Small curvature radii and stiff spheres in an environment with high values of the relative humidity behave like a DMT system.

All of the above discussion is valid if the deformation is purely elastic and in a quasistatic regime. In the case of sphere on a flat, the maximum pressure is exerted at the center of the contact area at a depth of $0.47r_c$.[29] Plastic deformation is initiated when the maximum pressure is equal to the yield stress value of the weakest material.[29] A good estimation of the yield stress can be obtained from the hardness value of the bulk. This value represents a lower limit, as it is quite likely that hardness increases for small volumes.[30,31] Therefore, in a specific case, it is possible to estimate whether a plastic deformation can occur by comparing the maximum pressure with the yield stress of the materials involved. As a first consideration it is important to stress that, if plastic deformation occurs, R^* tends to increase, which implies an increase of the contact area and, therefore, of the contact stiffness [Eq. (16)]. A second consideration is that the above evaluation is valid for the quasistatic case. Much more complex is to predict plastic deformation in the case of high strain rates such as UFM might be. In these cases extremely high pressure can be applied for short times to the contact (less than 0.1 μs for the UFM case). However, in most UFM applications this value decreases as occurs in the nonlinear regime when the tip moves away from the surface.[32] Up to now no extensive study has been undertaken to observe and measure plastic deformation on the nanoscale in such conditions. From a practical point of view, acquiring a topographical image of the investigated area can give an indication whether a plastic deformation has occurred and to what extent.

A further degree of complexity is added when performing dynamic measurements such as UFM. The problem of contact dynamics on the nanoscale is very complex and, to our knowledge, it has never been addressed systematically. However, it can be expected that viscoelasticity might play an important role, the more relevant the higher the modulation frequency. For instance, Maugis and Barquins[24] showed in a theoretical paper the possible variation that a JKR contact could undergo when one of the two bodies involved presents a viscoelastic behavior. Successive works have also pointed out an adhesion dependence on the approach-separation velocity.[33,34] In particular the adhesion hysteresis can be affected due to the fact that the point of instability at pull off depends on the viscoelastic properties of the two bodies. The presence of a water meniscus between the two bodies can also play an important role when performing dynamic measurements including possible variations of the point of instability at pull off. However, to our knowledge, direct studies of water meniscus dynamics as well as of a viscoelastic contact at high frequencies on the nanoscale have not yet been performed.

IV. SIMULATIONS

To check the applicability of the differential UFM, we have performed simulations of contact stiffness evaluation. We have assumed that there is no plastic or viscoelastic effect. Although this might not be true, it is a convenient starting point to gain insight in the technique. Furthermore, to our knowledge, models that include dynamical effects (such as viscoelasticity) have not been yet developed. A solid-solid contact described by the JKR model has been assumed. This model takes into account the adhesion force that acts between the tip and the surface and is generally considered realistic for AFM systems. Any other theoretical model of a solid-solid contact described in Sec. III can be taken, provided it has an analytical formulation.[35]

The ultrasonic deflection for two normal force values has been obtained (10 and 50 nN). The simulations of the cantilever deflection have been made using MATLAB (The Math Works, Inc.) and are divided in three main steps as described in the following.

(1) First of all a force-indentation curve $F(h)$ must be generated for a certain number of h values. The force-indentation curve is made of two branches: approach and retraction. To obtain the most general case, the force and the indentation are expressed in reduced units.

(2) The second step is to generate force-indentation curves modified by the ultrasonic modulation of the indentation. After choosing a value of indentation, the new force F_m is calculated for a set of ultrasonic amplitude values by using Eq. (1). The procedure is iterated for a set of indentation values. At this point, we have a two-dimensional matrix: one dimension is given by varying the initial indentation value, the other by varying the ultrasonic amplitude applied. Figure 5 shows the initial retraction branch and two modified retraction branches obtained at two different ultrasonic amplitude values. It can be noticed that the pull-off force and indentation values are modified and that F_m is generally higher than the force value at the corresponding indentation value for zero ultrasonic amplitude.

(3) In the third step, a cantilever spring constant value k_c and an initial normal force value F_1 are chosen. The force and the spring constant must be expressed in reduced units as already specified in step (1). Consequently the initial indentation h_1 can be calculated from the unmodified JKR retraction branch of step (1). Then Eq. (2) can be solved to obtain the new equilibrium indentation and normal deflection values at any given ultrasonic amplitude using the modified retraction branches calculated in step (2).

Figure 5 illustrates this solution. The straight line represents the Hooke law valid for the cantilever defined by

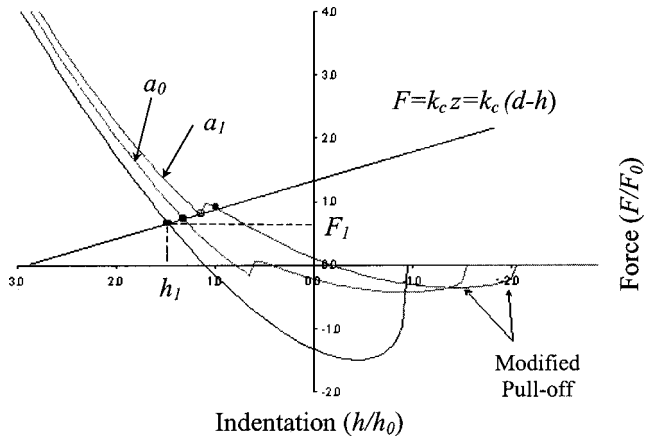

FIG. 5. The lowest curve represents the retraction branch of the force-indentation curve $F(h)$ for a JKR solid-solid contact. The force and the indentation are plotted in reduced units. The two other graphs represent the retraction branches modified by an out-of-plane ultrasonic vibration of the sample (Sec. IV). The ultrasonic amplitude values are sufficiently high to modify the pull-off force and indentation values ($a_1 > a_0$). The black line represents the Hooke law, which relates the force acting on the tip to the cantilever normal deflection z: $F(z)=k_c z=k_c(d-h)$ where k_c is the cantilever spring constant and d is the sample position. F_1 and h_1 are the initial normal force and indentation. The intersections between the black line and the modified retraction branches give the new equilibrium solutions of normal force and indentation values (filled circles). In particular, for a_1 (threshold amplitude) there are two solutions, one unstable (empty circle) and one stable (filled circle). The cantilever deflection undergoes a discontinuity (force jump).

choosing k_c and the initial force value F_1. The intersection between the line and the unmodified retraction branch (lower curve) gives the initial equilibrium solution of indentation and normal deflection values. The intersections between the line and the modified retraction branches give the new equilibrium solutions of indentation and normal deflection values (filled circles). In particular, the upper curve (a_1) corresponds to the ultrasonic amplitude at which there are two solutions, one unstable (open circle) and one stable (filled circle), and the cantilever deflection undergoes a discontinuity (threshold amplitude and force jump). In these simulations, the new equilibrium value of normal deflection is reached instantaneously.

At this point the threshold amplitude has been evaluated for the two normal force values and the effective contact stiffness calculated using Eq. (3). The procedure has been repeated for two different values of reduced Young's modulus and work of adhesion keeping constant all the other parameters ($R=50$ nm; $k_c=0.1$ N/m.) The results are reported in Table I along with the stiffness values according to the JKR model at $F_{\mathrm{av}}=30$ nN.

The stiffness values obtained via simulations of the differential UFM are in very good agreement with the JKR predictions. The error values are only due to discretization of the ultrasonic amplitude. These results give some confidence in the reliability of this method if the assumptions taken are valid.

V. EXPERIMENTAL APPARATUS

The experimental apparatus used for this work is based on a commercial AFM (Model CP, Park Scientific Instruments, 1171 Borregas Avenue, Sunnyvale, CA 94089). The system has been modified to implement UFM and to allow work under a controlled atmosphere.[32] Figure 6 shows a block diagram of the setup. The electronics, mechanics, and software of the commercial system will not be entirely described and one can refer to the manufacturer's manual for more details. We will only describe the features that are relevant to the understanding of the implementation of UFM.

The main mechanical modification is made to the sample holder to allow application of an out-of-plane ultrasonic vibration to the sample. The sample holder of the commercial system is a thin disk of metal. It is fixed to the piezoactuator through a magnet positioned inside the actuator. A piezoplate is glued to the sample holder with cyanoacrylate glue. For this work we have used piezoplates 1 mm thick and 1 or 2 cm in diameter. A piezoplate has a main longitudinal resonance that depends on its thickness (1 mm approximately gives 2 MHz and 0.1 mm gives 20 MHz). It also has other

TABLE I. Contact stiffness values obtained through the differential UFM by simulating the ultrasonic deflection at two values of normal force, 10 and 50 nN. Theoretical values of the JKR model at $F_{\mathrm{av}}=30$ nN are also reported. The reduced elastic modulus E_r and the work of adhesion $\Delta\gamma$ have been varied keeping constant all the other parameters: $R=50$ nm; $k_c=0.1$ N/m. The error values are only due to discretization of the ultrasonic amplitude.

E_r (GPa)	$\Delta\gamma$ (J/m^2)	Differential method (N/m)	JKR stiffness (N/m)
10	0.1	105 ± 10	114
10	1	189 ± 20	191
100	0.1	495 ± 40	520
100	1	872 ± 100	884

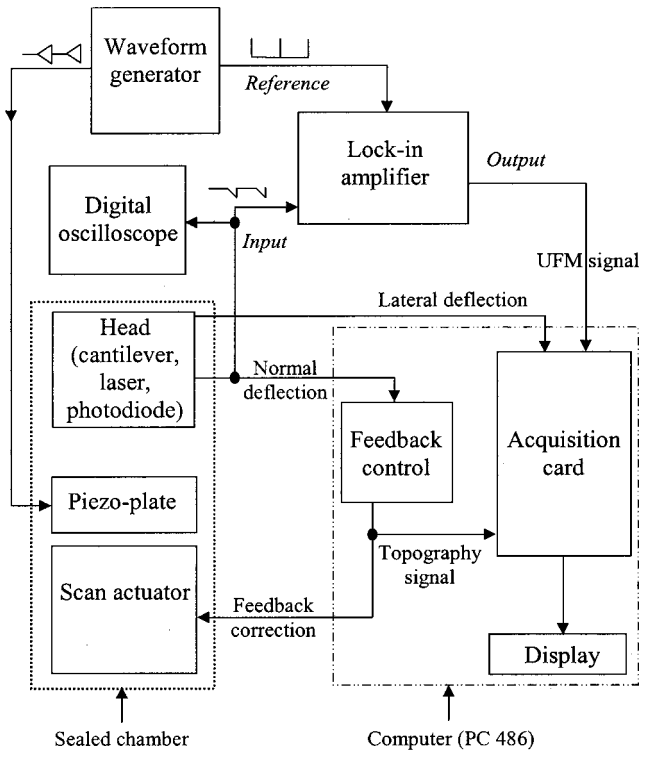

FIG. 6. Block diagram of the UFM experimental apparatus.

minor resonant modes at various frequencies (radial and other mixed modes). The out-of-plane displacement at nonresonant frequencies is quite small and, in general, not sufficient for exciting a nonlinear response. The sample is directly bonded to the piezoplate through an organic substance (salol, phenyl-salicylate) that melts at 70–80 °C. Salol provides a good binding that is needed for good ultrasound propagation. At the end of the experiment salol can be melted and the sample removed without any damage. Regarding the sample preparation there are some restrictions on the sample dimensions, depending on the AFM system used (2 cm maximum lateral dimensions), and weight. The specimen thickness must be generally smaller than the ultrasonic wavelength used for the experiments. For instance, a longitudinal ultrasonic wave of frequency of about 2 MHz (typically used in our experiments) has a wavelength of approximately 3 mm for ceramics and varies between 0.5–5 mm depending on the material.

To generate the ultrasonic vibration a programmable wave form generator is used (Hewlett Packard, Model 33120A, Arbitrary Waveform Generator). It can generate signals in a frequency range from 0.001 to 15 MHz. The amplitude can be modulated and the modulation shape can be set arbitrarily. The maximum output voltage is 10 Vpp on 50 Ω load and for a typical experiment an amplitude of 1–4 Vpp is applied to the piezoplate. The modulated voltage is applied to the piezoplate via a small connection fixed on the AFM head. One can also add in parallel an inductive coil with a low loss Hartree-Fock ferrite toroidal core in order to match the impedance of the piezoplate to the impedance of the wave-form generator output.

The commercial electronics and acquisition system are generally quite flexible and allow access to internal signals such as normal and lateral deflections and feedback error signal. The ultrasonic deflection can be visualized by using the feedback error signal. The feedback error signal is fed into a digital oscilloscope and monitored alongside with the ultrasonic signal applied to the piezoplate. The digital oscilloscope (Stanford Research System, Model SR830 DSP lock-in amplifier) allows averaging of the signal up to 256 times. The oscilloscope display can be printed out or acquired via computer so that the normal deflection signal can be analyzed afterwards in order to evaluate the threshold amplitude. However this acquisition, done with an external software application, cannot be used to sample the ultrasonic deflection at each point of a scan due to slow acquisition rate.

In Sec. IV it has been pointed out that one of the main assumptions of UFM is that the cantilever does not follow the ultrasonic vibration applied to the sample. It would be very important to verify this assumption. But at the moment it is not possible to obtain normal deflection spectra of the cantilever in the desired bandwidth of 3 MHz.

In order to control the relative humidity (RH), the AFM hardware has been placed in an acrylic chamber that has a lid with dry nitrogen and vacuum pump inlets on top of it. To reduce the RH, P_2O_5 powder and flux of dry nitrogen are used; to increase the RH water is introduced. The chamber has proved to be reasonably sealed, so that the minimum RH achievable is about 15%. The upper limit is set by the tolerance of the electrical connections of the commercial machine to RH and it is around 75%.

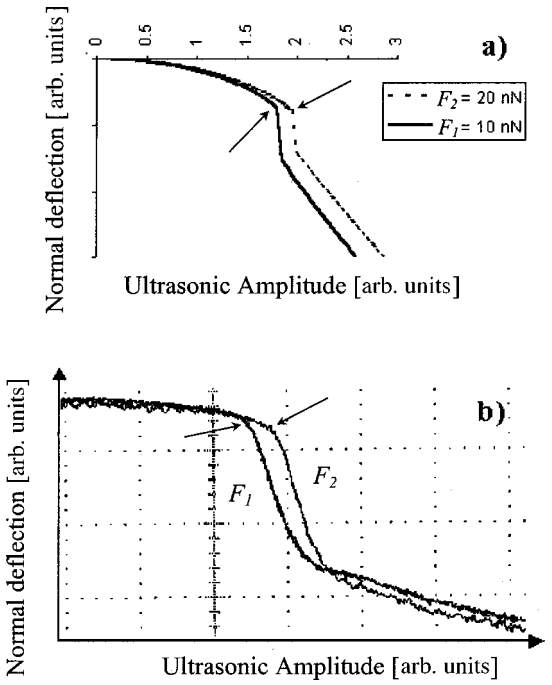

FIG. 7. (a) Simulations of the ultrasonic deflection for two normal force values. The ultrasonic vibration is ramped in amplitude. A JKR solid-solid contact is assumed for the tip-surface interaction. Arrows indicate the reaching of the pull-off point at which the contact is first broken. (b) Experimental signals of the ultrasonic deflection under the same conditions assumed for the theoretical simulations (silicon tip and sample, normal force values, cantilever spring constant). The reaching of the pull-off point is not as clear as for the simulated curves. This is due to the fact that the cantilever does not react instantaneously. The dependence of the threshold amplitude on the normal force is qualitatively in agreement.

VI. DESCRIPTION OF THE EXPERIMENTAL PROCEDURES

Before proceeding with the description of the experimental procedures a few considerations must be taken regarding the cantilever response to the ultrasonic force. In Fig. 7 simulated and experimental ultrasonic deflection signals have been reported for two normal force values.[32] As the theory predicts, in the experimental curves there is a force jump after an initial slight nonlinear response. Thereafter the normal deflection increases almost linearly. The ultrasonic amplitude at which the force jump occurs depends on the normal force. Thus under the assumptions stated above, the stiffness can be evaluated from the experimental data using Eq. (3). It has to be noted that the cantilever response is not instantaneous and the force jump at pull off produces a sharp slope but not a discontinuity. However it has been observed that for a given cantilever this sharp slope does not depend on the initial normal force. Therefore, although the evaluation of the absolute value of the threshold amplitude can be affected, Δa is not. For the same reason the cantilever takes a finite time to reach the rest position after the ultrasonic amplitude is set to zero at the end of the amplitude modulation cycle. It is extremely important that one allows the can-

tilever to reach the rest position before starting to newly increase the ultrasonic amplitude, otherwise the evaluation of Δa could be affected.

Preliminary experiments were carried out on a variety of materials over a range of normal forces between -10 and 30 nN. The measurements were performed at one single point, i.e., no scan was performed, in order to reduce any influence of shear and topography. The cantilevers used were the V-shaped silicon cantilevers available commercially with a spring constant between 0.18–0.24 N/m and a nominal tip radius of 10 nm (Ultralever™, Park Scientific Instruments). The samples were either freshly cleaved or rinsed in acetone and then introduced in a controlled environment. The time elapsed between cleaning or cleaving and the experiment quite often exceeded 1 h. No precaution was taken in this respect. Furthermore, for this set of experiments, the ultrasonic amplitude calibration was performed using an indirect method.[10] This calibration was carried out by increasing the ultrasonic amplitude and assuming that the increase rate of the normal deflection at amplitude much larger than the force jump was equal to the increase rate of the ultrasonic amplitude. Thus one could calibrate the ultrasonic amplitude, providing the cantilever deflection signal was calibrated.

On comparison with continuum mechanics theoretical models, it was found that the experimental values of contact stiffness were almost one order of magnitude smaller than the theoretical values. After a detailed analysis of these preliminary results, two hypotheses were put forward to explain the discrepancies between experimental and theoretical values: either a solid-solid contact did not take place due to contamination, or the ultrasonic amplitude calibration was not correct. Therefore two precautions were taken in later experiments: (a) careful cleaning of tip and sample; (b) ultrasonic amplitude calibration since the indirect calibration method proved unreliable on careful examination. A new homodyne interferometer was built.[32] Thereafter the stiffness measurements were done referenced to a calibrated ultrasonic amplitude.

A third important issue regarded the range of the normal force values. Our commercial apparatus does not allow one to work above a certain normal deflection value. This is probably because the laser spot would fall outside the photodiode or the linear relation between cantilever normal deflection and normal force would not be valid. Therefore, in order to work at normal force values higher than 30 nN, one needs to use stiffer cantilevers. In particular if the cantilever spring constant is 2.8 N/m, the normal force range can be extended up to 300 nN. In this way the contact stiffness can be measured over a broad enough range of normal force. Data can then be compared to the predictions of the theoretical models. Such comparison is crucial in order to understand the nature of the contact.

The samples were chosen so that the topography was reasonably smooth with wide homogeneous areas. Typically an AFM topographical image was acquired before and after the UFM experiments. This was done not only to avoid any possible topographical artifact but also because one entire acquisition can last 15–20 min on average. In an ambient environment thermal drifts are unavoidable, so that there is always a lateral movement of the tip relative to the surface and at the end of the experiment the tip is not on the initial position. Experiments should be started after thermalizing the system so that the thermal drift is minimized. However, the thermalization time must not be too long as the tip and the sample become contaminated. The commercial system itself is not temperature stabilized. A compromise thermalization time must therefore be found. For these experiments it was around 5–10 min.

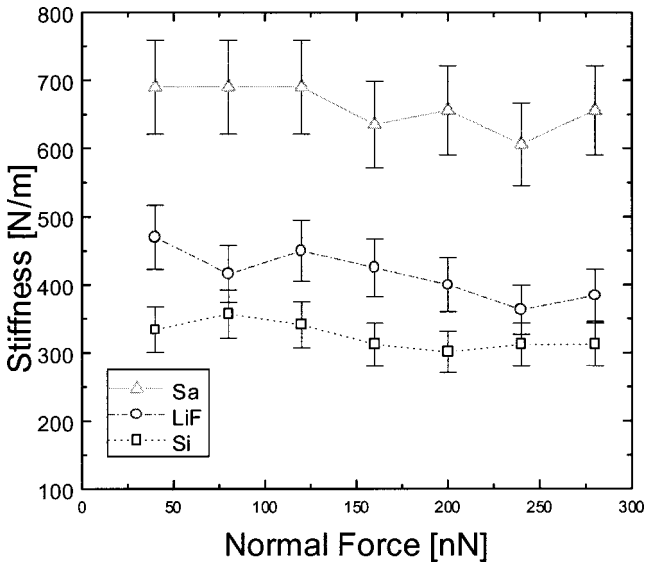

FIG. 8. Experimental data for three materials: sapphire, silicon (100), and LiF (100). The samples were probed with the same V-shaped silicon cantilever (nominally $k_c = 2.8$ N/m, $R = 10$ nm). The surface rms roughness is less than 0.2 nm over a few μm^2 for all the three samples. The slope of all the three curves is approximately null. The relative difference between the three sets of data reveals that the differential UFM can distinguish materials on the basis of their elastic properties.

VII. RESULTS

In Fig. 8 we present data resulted from an investigation of three different samples with different elastic properties. A silicon V-shaped cantilever was employed (nominally $k_c = 2.8$ N/m, $R = 10$ nm). The three materials were sapphire, silicon (100), and lithium fluoride LiF (100). Silicon and sapphire were carefully cleaned in soap, acetone, methanol, and sonicated for 5 min at each step; the lithium fluoride was freshly cleaved before the measurements. The Young's moduli of sapphire, silicon, and LiF are 380 GPa,[36] 165 GPa,[37] and 106 GPa,[36] respectively. The materials were investigated in the following order: sapphire, LiF, and silicon. Sapphire presented higher stiffness as expected. In spite of having a higher Young's modulus, the silicon sample turned out to be more compliant than the LiF sample. This could be attributed to the presence of a native oxide layer ($E_{SiO_2} = 71$ GPa).[36] In all three cases, the slope of the curve is approximately zero.

In an ambient environment, a parameter that might influence the nanocontact is the RH. In fact the shape of the water meniscus strongly depends on the RH value. We therefore studied the influence of RH on the contact stiffness. In our experimental apparatus, the RH can only be reduced to a minimum value of 18%. The upper limit is around 75%. A

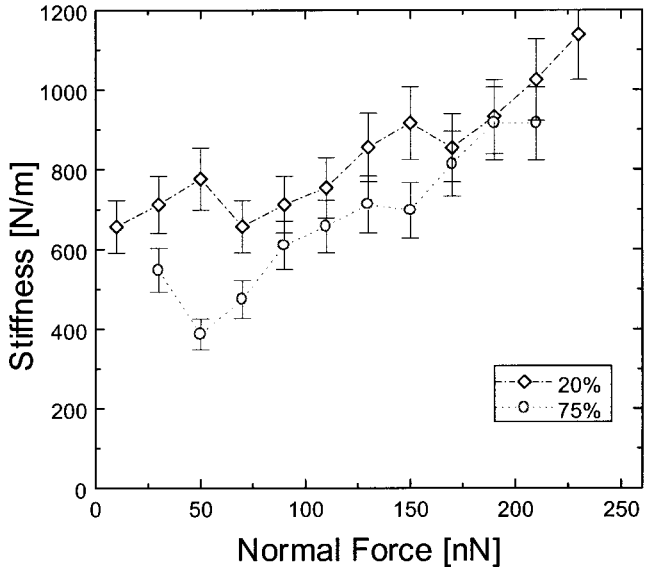

FIG. 9. Stiffness measurements on a sapphire sample varying the relative humidity (RH). A silicon V-shaped cantilever was employed (nominally $k_c = 2.8$ N/m, $R = 10$ nm). The contact stiffness generally increases with increasing normal force. At a lower RH value the contact stiffness is higher. This observation is in accordance with another set of data that was recorded at a low normal force value. Independently of the RH value, the contact stiffness seems to be similar at high normal force values.

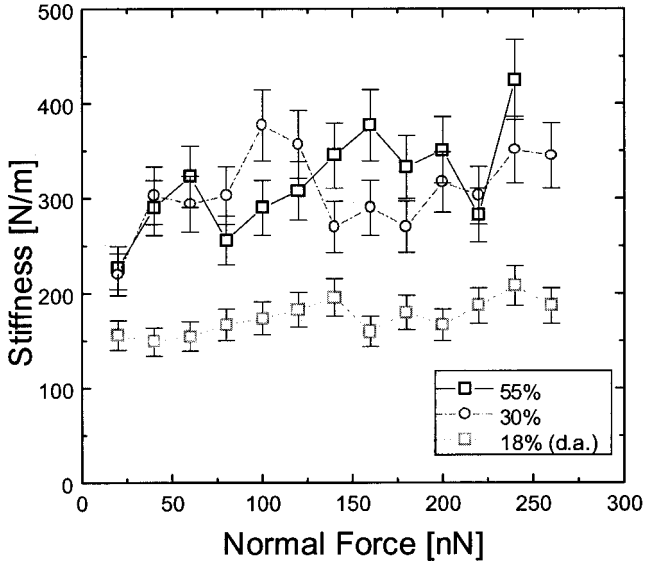

FIG. 10. Stiffness measurements on a silicon (100) sample varying the RH. A silicon V-shaped cantilever was employed (nominally $k_c = 2.8$ N/m, $R = 10$ nm). For the two sets of measurements at 30% and 55% of RH, no clear dependence on RH is noticeable. The slope shows a general increase in stiffness with increasing normal force. A set of data taken 1 day later at 18% RH shows stiffness values of a factor of 2 smaller. This was probably due to the presence of contamination of the sample. At 70% RH the ultrasonic deflection signal was quite unstable: the results were variable with time and were not reproducible.

long period of time is needed to change the RH value and this is a significant limit as we shall see. In Figs. 9 and 10, data for sapphire and silicon at various RH values are presented. Both samples were investigated with a silicon V-shaped cantilever (nominally $k_c = 2.8$ N/m, $R = 10$ nm). In this case silicon was investigated first.

Starting with sapphire (Fig. 9), the two sets of data were taken at two extreme values, 20% and 75% RH. The signal was stable and the results reproducible (no appreciable variation in the threshold amplitude when reducing the normal load). The two plots show that stiffness increases with increasing normal force. Figure 9 also shows that at a lower RH value the contact stiffness is higher. This dependence on RH is in accordance with another set of data that was recorded at a low normal force value. Independently of the RH value, the contact stiffness seems to tend to similar values at high normal force. With the silicon data (Fig. 10), the situation is slightly different. Data were taken at two different values of RH (30% and 55%). As for the case of sapphire, the contact stiffness generally increases with increasing normal load but no clear dependence on RH is noticeable. At 70% RH the ultrasonic deflection signal became unstable: the results were variable with time and were not reproducible. No plausible explanation has been found. A set of data taken 1 day later at 18% RH shows that stiffness decreased by a factor of 2. This observation might be explained by the presence of contamination on the surface that reduces the contact stiffness. A similar effect has been already mentioned in the previous section.

As a final observation we would like to mention that several experiments were interrupted as the normal deflection signal suddenly became unstable. This could suggest that the tip might undergo deformations during the application of ultrasound. Therefore we took scanning electron microscopy (SEM) images of the tip used for the measurements on silicon and sapphire varying the RH value. We have noticed that the overall shape of the tip can be modified becoming blunter with respect to the tip shape before UFM measurements. It is difficult to identify the exact moment at which the tip is modified. However these results indicate that the application of an out-of-plane ultrasonic vibration could lead to a change of the tip shape. This change can be detected sometimes. For a set of measurements carried out on sapphire at 30% RH, data were scattered and did not present a definite trend. This was probably due to small modifications of the tip apex. In fact the ultrasonic deflection was subjected to small but noticeable variations.

VIII. DISCUSSION

Let us first consider the sets of data presented in Fig. 8. All the curves show no dependence of the contact stiffness on the normal force. On the contrary, the continuum mechanics models predict an increase of contact stiffness with increasing normal force. However, in these experiments, the actual shape of the tip employed may be different from the spherical one usually assumed. On the basis of the following equation:[38]

$$S = 2E_r\sqrt{A/\pi}, \tag{21}$$

valid for a Hertzian contact between a flat surface and an axisymmetric probe, no dependence of the contact stiffness on the normal force is expected if the tip apex was represented by a flat punch. In this case, sapphire, which is the

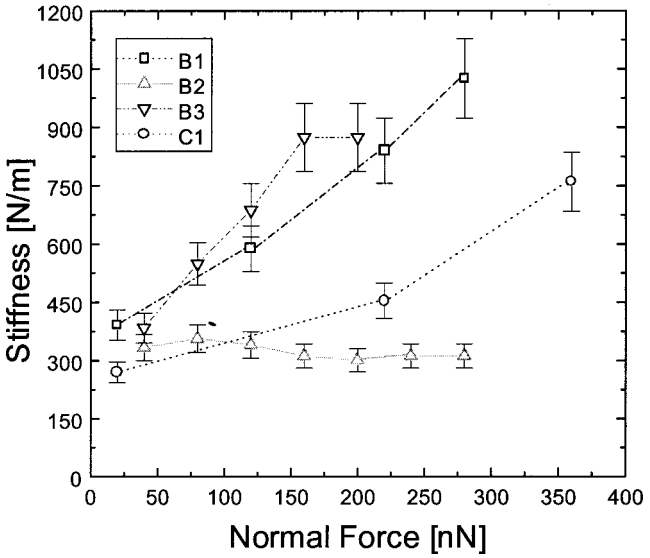

FIG. 11. Experimental data for a silicon (100) surface. Four different silicon tips have been used mounted on cantilevers with two different spring constant values. The sample rms roughness was less than 0.2 nm over a few μm^2. This high value is mainly determined by noise. The four graphs are quite different in their overall shape. One is relatively flat over the whole range of normal force values. The other three show an increase of the contact stiffness with increasing normal force, but with somewhat different slopes.

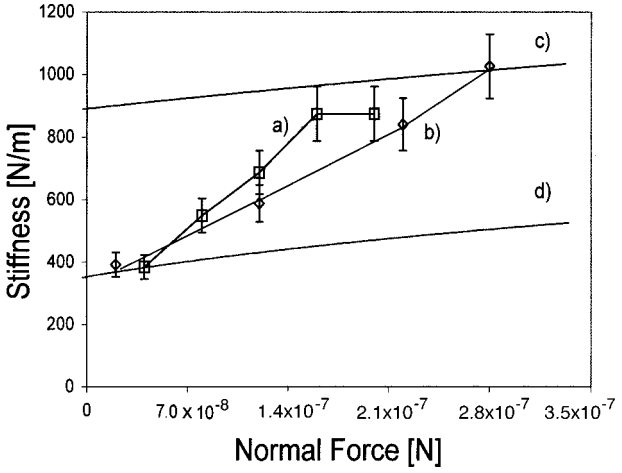

FIG. 12. (a), (b) Two sets of experimental data on silicon (Fig. 11) are compared with (c),(d) JKR curves. The Young's modulus value was set to 165 GPa, the surface energy to 1.4 J/m^2. Two theoretical curves have been plotted using different tip radius values: 6 and 25 nm. The experimental values at low normal forces match the theoretical values calculated assuming a tip radius of 6 nm. On the other hand, at high normal forces, they tend to be in agreement with the theoretical values obtained assuming a tip radius of 25 nm.

stiffest material, was first investigated and this might have contributed to a flattening of the tip. The fact that most of the other sets of data taken for silicon (Fig. 11) have different slopes could be a further hint suggesting that the tip was flat or a shape modification may have occurred previously to the data acquisition. A SEM investigation of the tip used after the three sets of experiments suggested that the tip radius of curvature is larger than the nominal value of 10 nm. Although the perspective was not ideal and it is difficult to see the actual shape of the tip apex, the hypothesis of a flat punch could not be ruled out. Independently of the tip shape, the relative difference between the three sets of data of Fig. 8 reveals that the differential UFM can distinguish materials on the basis of their elastic properties. Calculations made using Eq. (21) and assuming for E_r [Eq. (7)] the bulk values of the three materials investigated have given the same value of $\sqrt{A}=5$ nm in all three cases with a spread of $\pm 2\%$.

In Fig. 11 we have plotted other results obtained for silicon using four different silicon tip-cantilever systems. These sets of measurements were carried out in an ambient environment at 20 °C and 30–40 % of RH. The four graphs are quite different in their overall shape. The one already reported in Fig. 8 is relatively flat over the whole range of normal force values. The other three show an increase of the contact stiffness with increasing normal force, but with somewhat different slopes. These differences should be attributed to differences in tip shape. A flat tip gives a curve with no slope and a spherical tip a curve with a positive slope. However, discrepancies between the experimental data and the theoretical predictions still remain as shown in Fig. 12 for a JKR model (the same is valid for DMT and generalized Hertzian models).

To explain these discrepancies, three hypotheses have been put forward.

(1) The tip apex deforms and its radius of curvature continuously increases when the normal force is increased.

(2) A compliant layer of finite thickness is interposed between the tip and the surface affecting the contact stiffness dependence on the normal force.

(3) Viscoelasticity might play an important role at such high-frequency modulation.

The first hypothesis cannot be checked directly with the available instrumentation. The maximum pressure calculated for silicon on sapphire at a force of 300 nN with a tip radius of 10 nm is equal to 9 GPa. On the other hand, the maximum pressure is equal to 6 GPa for silicon on silicon at a force of 300 nN with a tip radius of 10 nm. These values decrease by increasing the tip radius. Hardness values for sapphire and silicon are 28 GPa (Ref. 38) and 20 GPa,[30] respectively. Therefore, in quasistatic approximation, a plastic deformation might be just initiated in the silicon body in the case of sapphire and silicon at 300 nN and a tip radius of 10 nm. The fact that in UFM operation a high strain rate is applied further induces us to consider the possibility of a plastic deformation. It has been reported that the dynamic pressure can increase up to a factor of 2 the static pressure at the initially set normal force. However, in the nonlinear detection regime, the tip moves away from the surface and, therefore, the contact pressure reaches high values only for a few cycles and for a short period of time. For these sets of measurements, the ultrasonic deflection and stiffness values at low loads were reproducible when the normal force was decreased after measurements carried out at high normal force values. Besides, topographical images did not show any clear deformation imputable to plastic deformation. Another interesting observation is that the pull-off force did not appreciably vary after each set of measurements. Therefore if plastic deformation occurred, this effect was not dramatic though it might still be relevant for the interpretation of our results.

The second hypothesis is based on studies that report liq-

uid layering when squeezed between tip and surface.[39–41] Though for water no clear observation of such behavior has been reported, there is some evidence that this solid transition might occur. If this happened, a cushion relatively more compliant than the two surfaces might interpose between the two bodies reducing the contact stiffness. As the normal load gradually increases this cushion could either stiffen or disappear giving rise to a solid-solid contact.

The third hypothesis is also quite relevant. However, it is objectively very difficult to implement any experiment to verify it. In Sec. III, it has been already pointed out that JKR and other continuum mechanics models are valid in a quasistatic regime and might not be valid in a dynamic regime such as in UFM. Viscoelasticity might influence the shape of the force-indentation curve (pull-off point, adhesion hysteresis, etc.). However, it is difficult to predict what effect this might produce on the stiffness evaluation and its dependence on the normal load.

Let us now consider the results obtained varying the relative humidity. It is firstly to be noticed that the ratio of contact stiffness for sapphire and silicon at the same load is approximately equal to the one calculated from the experimental data presented in Fig. 8. This is further evidence that materials with different Young's moduli can be distinguished using the differential UFM. Other considerations regard the slope of the stiffness-load curves, which is not in agreement with the theoretical predictions, and the fact that by changing the RH value, the curves are shifted to lower values. As for the sets of measurements previously analyzed, the ultrasonic deflection and stiffness values at low loads were reproducible when the normal force was decreased after measurements carried out at high loads. Topographical images did not show any clear deformation and the pull-off force did not appreciably vary after each set of measurements. Therefore, we are again left with two hypotheses: the presence of a compliant layer between the two bodies in contact; continuum mechanics models might not be valid in a dynamic regime such as in UFM. These hypotheses will be the subject of future studies.

IX. CONCLUSIONS

The differential UFM has been applied to materials of various elastic properties in different environmental conditions. It has proved to be capable of measuring absolute stiffness values of nanoscale contacts up to 1000 N/m. This is achieved by using relatively compliant cantilevers (2.8 N/m). Materials with different elastic constants such as sapphire, LiF, and silicon have been successfully differentiated. The results obtained show that the tip shape might play an important role: for instance, a blunt tip would give no dependence of the stiffness on the normal force. The environmental conditions and the surface state are also quite influential factors. Not clean surfaces can induce lowering of the contact stiffness whereas high relative humidity can lower the contact stiffness and sometimes induce instabilities in the UFM detection.

While continuum mechanics models provide stiffness values of the same order of the measured values, they cannot explain the dependence of contact stiffness on the normal force and on the relative humidity. This can be due to the fact that these models are valid in quasistatic approximation and in a clean environment, while UFM operates at very high vibration frequencies in an ambient environment. In this high-frequency regime, it is likely that viscous forces might play an important role modifying the force-indentation curve. Plastic deformation might also occur due to the high strain rates. Another possible cause of the discrepancies might be the presence of water in between the two bodies in contact. Nevertheless, it can be concluded that using the UFM approach it is possible to advance into the unexplored area of the submicrosecond dynamics of nanometer contacts.

ACKNOWLEDGMENTS

F.D. and O.V.K would like to thank the Paul Instrument Fund and EPSRC support (GR/L02234) for the development of UFM. F. D. would like to thank the ''AFAM'' CEC Network for financial support.

*Present address: Department of Chemical Engineering, University of Washington, P.O. Box 351750, Seattle, WA 98195.
†On leave from Symyx Technologies, 3100 Central Expressway, Santa Clara, CA 95051.

[1] G. Binnig, C. F. Quate, and C. Gerber, Phys. Rev. Lett. **56**, 930 (1986).
[2] D. Rugar and P. K. Hansma, Phys. Today **43** (10), 23 (1990).
[3] P. Maivald, H.-J. Butt, S. A. C. Gould, C. B. Prater, and B. Drake *et al.*, Nanotechnology **2**, 103 (1991).
[4] M. Radmacher, R. W. Tilmann, and H. E. Gaub, Biophys. J. **64**, 735 (1993).
[5] N. A. Burnham, J. Vac. Sci. Technol. B **12**, 2219 (1994).
[6] S. P. Jarvis, A. Oral, T. P. Weihs, and J. B. Pethica, Rev. Sci. Instrum. **64**, 3515 (1993).
[7] E.-L. Florin, M. Radmacher, B. Fleck, and H. E. Gaub, Rev. Sci. Instrum. **65**, 639 (1994).
[8] S. P. Jarvis, S.-I. Yamamoto, H. Yamada, H. Tokumoto, and J. B. Pethica, Appl. Phys. Lett. **70**, 2238 (1997).
[9] W. Rohrbeck and E. Chilla, Phys. Status Solidi A **131**, 69 (1992).
[10] O. Kolosov and K. Yamanaka, Jpn. J. Appl. Phys., Part 2 **32**, L1095 (1993).
[11] N. A. Burnham, A. J. Kulik, G. Gremaud, P.-J. Gallo, and F. Ouveley, J. Vac. Sci. Technol. B **14**, 794 (1996).
[12] U. Rabe and W. Arnold, Ann. Phys. **3**, 589 (1994).
[13] N. A. Burnham and R. J. Colton, J. Vac. Sci. Technol. A **7**, 2906 (1989).
[14] N. A. Burnham, G. Gremaud, A. J. Kulik, P.-J. Gallo, and F. Ouveley, J. Vac. Sci. Technol. B **14**, 1308 (1996).
[15] K. Yamanaka, H. Ogiso, and O. Kolosov, Appl. Phys. Lett. **64**, 178 (1994).
[16] U. Rabe, K. Janser, and W. Arnold, Rev. Sci. Instrum. **67**, 3281 (1996).
[17] S. Hirsekorn, U. Rabe, and W. Arnold, Nanotechnology **8**, 57 (1997).
[18] J. B. Pethica and W. C. Oliver, in *Thin Films: Stresses and Mechanical Properties*, edited by M. E. Gross, J. Jasinki, and J. T. Yates, Jr., MRS Symposium Proceedings No. 130 (Materials Research Society, Pittsburgh, 1989).
[19] H. Hertz, J. Reine Angew. Math. **92**, 156 (1882).
[20] J. Boussinesq, *Application des Potentiels a L'etude de L'equilibre et du Movement des Solides Elastiques* (Gauthier Villars, reed. Blanchard, Paris, 1885).

[21] K. L. Johnson, K. Kendall, and D. Roberts, Proc. R. Soc. London, Ser. A **324**, 301 (1971).
[22] B. V. Derjaguin, V. M. Muller, and Y. P. Toporov, J. Colloid Interface Sci. **53**, 314 (1975).
[23] V. M. Muller, V. S. Yushenko, and B. V. Derjaguin, J. Colloid Interface Sci. **92**, 92 (1983).
[24] D. Maugis and M. Barquins, J. Phys. D **11**, 1989 (1978).
[25] J. N. Israelachvili, *Intermolecular and Surface Forces*, 2nd ed. (Academic, Suffolk, United Kingdom, 1995).
[26] D. Maugis, J. Colloid Interface Sci. **150**, 243 (1992).
[27] A. L. Weisenhorn, P. K. Hansma, T. R. Albrecht, and C. F. Quate, Appl. Phys. Lett. **54**, 2651 (1989).
[28] A. Fogden and L. R. White, J. Colloid Interface Sci. **138**, 414 (1990).
[29] B. Bhushan and A. V. Kulkarni, Thin Solid Films **278**, 49 (1996).
[30] J. B. Pethica, R. Hutchings, and W. C. Oliver, Philos. Mag. A **48**, 593 (1983).
[31] M. S. Bobji, S. K. Biswas, and J. B. Pethica, Appl. Phys. Lett. **71**, 1059 (1997).
[32] F. Dinelli, Ph.D. thesis, Oxford, 1999.
[33] J. A. Greenwood and K. L. Johnson, Philos. Mag. A **43**, 697 (1981).
[34] K. L. Johnson and H. M. Pollock, J. Adhes. Sci. Technol. **8**, 1 (1994).
[35] K. Yamanaka, H. Ogiso, and O. Kolosov, Jpn. J. Appl. Phys., Part 1 **33**, 3197 (1994).
[36] G. A. D. Briggs, *Acoustic Microscopy* (Oxford University Press, New York, 1992).
[37] R. M. Overney and E. Meyer, MRS Bull. **18**, 26 (1993).
[38] G. M. Pharr, W. C. Oliver, and F. R. Brotzen, J. Mater. Res. **7**, 613 (1992).
[39] R. G. Horn and J. N. Israelachvili, J. Chem. Phys. **75**, 1400 (1981).
[40] J. N. Israelachvili and R. M. Pashley, Nature (London) **306**, 249 (1983).
[41] S. J. O'Shea, M. E. Welland, and T. Rayment, Appl. Phys. Lett. **60**, 2356 (1992).